ACCOUNTS
of chemical research

Polycrystallinity and Stacking in CVD Graphene

ADAM W. TSEN,[†] LOLA BROWN,[‡] ROBIN W. HAVENER,[†] AND JIWOONG PARK*[,‡,§]

[†]*Department of Applied Physics,* [‡]*Department of Chemistry and Chemical Biology, and* [§]*Kavli Institute at Cornell for Nanoscale Science, Cornell University, Ithaca, New York 14853, United States*

RECEIVED ON JULY 3, 2012

CONSPECTUS

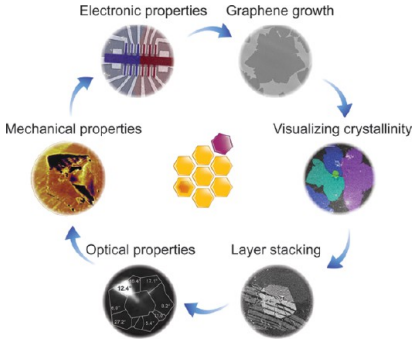

Graphene, a truly two-dimensional hexagonal lattice of carbon atoms, possesses remarkable properties not seen in any other material, including ultrahigh electron mobility, high tensile strength, and uniform broadband optical absorption. While scientists initially studied its intrinsic properties with small, mechanically exfoliated graphene crystals found randomly, applying this knowledge would require growing large-area films with uniform structural and physical properties. The science of graphene has recently experienced revolutionary change, mainly due to the development of several large-scale growth methods. In particular, graphene synthesis by chemical vapor deposition (CVD) on copper is a reliable method to obtain films with mostly monolayer coverage. These films are also polycrystalline, consisting of multiple graphene crystals joined by grain boundaries. In addition, portions of these graphene films contain more than one layer, and each layer can possess a different crystal orientation and stacking order.

In this Account, we review the structural and physical properties that originate from polycrystallinity and stacking in CVD graphene. To begin, we introduce dark-field transmission electron microscopy (DF-TEM), a technique which allows rapid and accurate imaging of key structural properties, including the orientation of individual domains and relative stacking configurations. Using DF-TEM, one can easily identify "lateral junctions," or grain boundaries between adjacent domains, as well as "vertical junctions" from the stacking of graphene multilayers. With this technique, we can distinguish between oriented (Bernal or rhombohedral) and misoriented (twisted) configurations.

The structure of lateral junctions in CVD graphene is sensitive to growth conditions and is reflected in the material's electrical and mechanical properties. In particular, grain boundaries in graphene grown under faster reactant flow conditions have no gaps or overlaps, unlike more slowly grown films. These structural differences can affect the material's electrical properties: for example, better-connected grain boundaries are more electrically conductive. However, grain boundaries in general are mechanically weaker than pristine graphene, which is an order of magnitude stronger than CVD graphene based on indentation measurements performed with an atomic force microscope.

Vertical junctions in multilayer CVD graphene have two key structural features. First, bilayer graphene (BLG) with Bernal stacking exists in two mirrored configurations (AB or AC) that also form isolated domains. Similarly, oriented trilayer graphene also has alternating ABA and ABC stacked layers. Second, in twisted multilayer graphene, stacked layers lack long-range atomic registry and can move freely relative to each other, which generates unique optical properties. In particular, an interlayer optical excitation produces strong Raman and absorption peaks, dependent on the twist angle.

A better understanding of the structural and physical properties of grain boundaries and multilayers in CVD graphene is central to realizing the full potential of graphene in large-scale applications. In addition, these studies provide a model for characterizing other layered materials, such as hexagonal boron nitride and MoS_2, where similar polycrystallinity and stacking are expected when grown in large areas.

Introduction

Ever since the discovery that single atomic layers of graphite can be stably isolated using mechanical exfoliation, there has been an explosive effort to investigate the various properties of two-dimensional graphene.[1] Consisting of a monolayer of hexagonally bonded carbon atoms, the unique crystalline structure of graphene gives rise to a host of exceptional characteristics. Electronically, its band-structure

Published on the Web 11/07/2012 www.pubs.acs.org/accounts
10.1021/ar300190z

in reciprocal space resembles that of massless relativistic particles and allows carriers to move with extremely high mobility with little scattering even in ambient conditions.[2] Optically, graphene's band structure enables it to absorb roughly 2% of broadband light, a surprisingly large value for an atomically thin material.[3] Mechanically, graphene's intrinsic strength is predicted to be greater than that of any other material due to the large energies of its covalent carbon–carbon bonds.[4]

In order to exploit such outstanding properties, researchers have undertaken to integrate graphene into a broad variety of relevant technological applications. Unfortunately, the simple exfoliation of graphene that initiated the field could not satisfy the size and scale requirements for these efforts,[1] and so several methods have been developed to obtain large-area graphene with greater throughput. For instance, large-scale graphene with high electronic performance can be grown epitaxially on silicon carbide.[5] Such samples are mechanically coupled to the semiconducting substrate, however, although it can be doped to decouple the graphene electronically.[6] In contrast, the self-assembly of graphene oxide sheets and their subsequent reduction could provide a low-cost, water-soluble alternative,[7] but such films also tend to exhibit poor electrical conductivity, limiting their potential applications. Recently, graphene synthesis by chemical vapor deposition (CVD) on copper has emerged as one of the most convenient techniques to obtain high-quality, single-layer graphene, which can then be transferred to arbitrary substrates using a simple etching process.[8−12] Furthermore, this method is scalable and has been used to produce films on even meter length scales.[13] A schematic of the growth process is shown in Figure 1A.[14]

When materials are assembled in macroscopic sizes involving billions of atoms, however, their homogeneity becomes an important issue. For the case of CVD graphene, this can be clearly understood from Figure 1B, which shows a scanning electron microscopy (SEM) image of graphene which was grown to only partially cover the underlying copper surface. Here, we see that graphene has nucleated at multiple sites and grown to form island structures. In general, each island may consist of one or more crystal orientations distinct from its neighbors, and as a result their intersections will form defect structures known as grain boundaries. The presence of grain boundaries in polycrystalline graphene films could potentially alter their behavior, as theoretically they are predicted to have unique electronic,[15] mechanical,[16,17] and chemical properties,[18] deviating from those of the pristine graphene lattice.

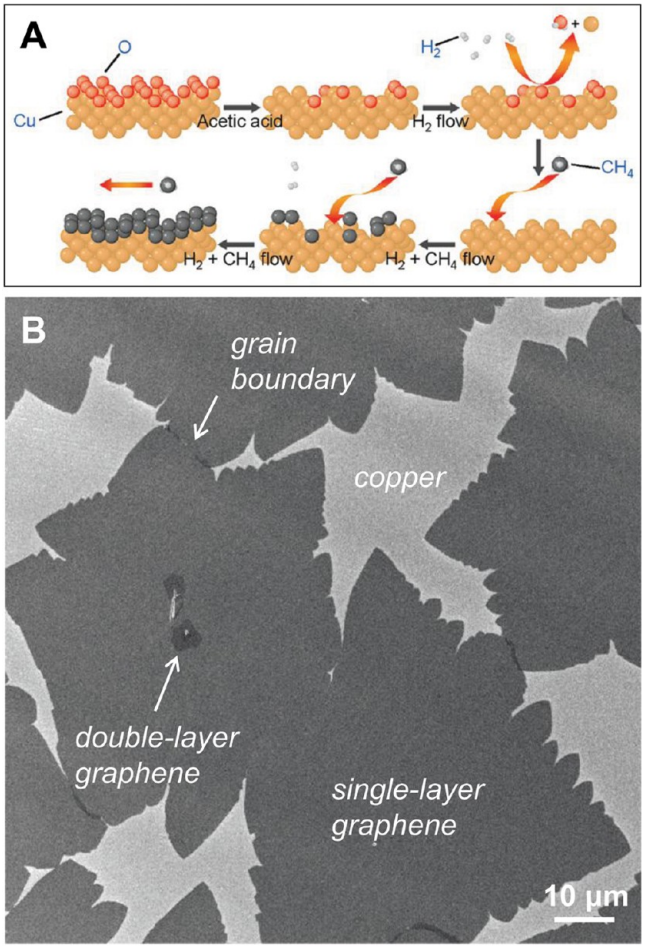

FIGURE 1. Graphene CVD synthesis. (A) Schematic of CVD graphene growth on copper. Reproduced with permission from ref 14. Copyright 2009 American Chemical Society. (B) SEM image of partially grown graphene on Cu foil.

Within the islands, we also observe that a second graphene layer has grown locally. While their size and frequency of formation may be tuned by changing growth conditions,[19] the synthesis of multilayered graphene introduces additional degrees of freedom, as each individual layer may also possess a different crystal orientation from those directly above and below. These variations in layer orientation and stacking order are also expected to induce distinct physical properties. For instance, bilayer graphene (BLG) that is Bernal-stacked was shown to possess an electronic bandgap tunable with the application of a vertical electric field, whereas twisted BLG is expected to show completely decoupled low-energy electronic states for large rotation angles.[20]

In this Account, we will describe recent results aimed at understanding the effects of polycrystallinity and stacking order in CVD graphene films. We will discuss the morphology of individual grain boundaries formed during CVD

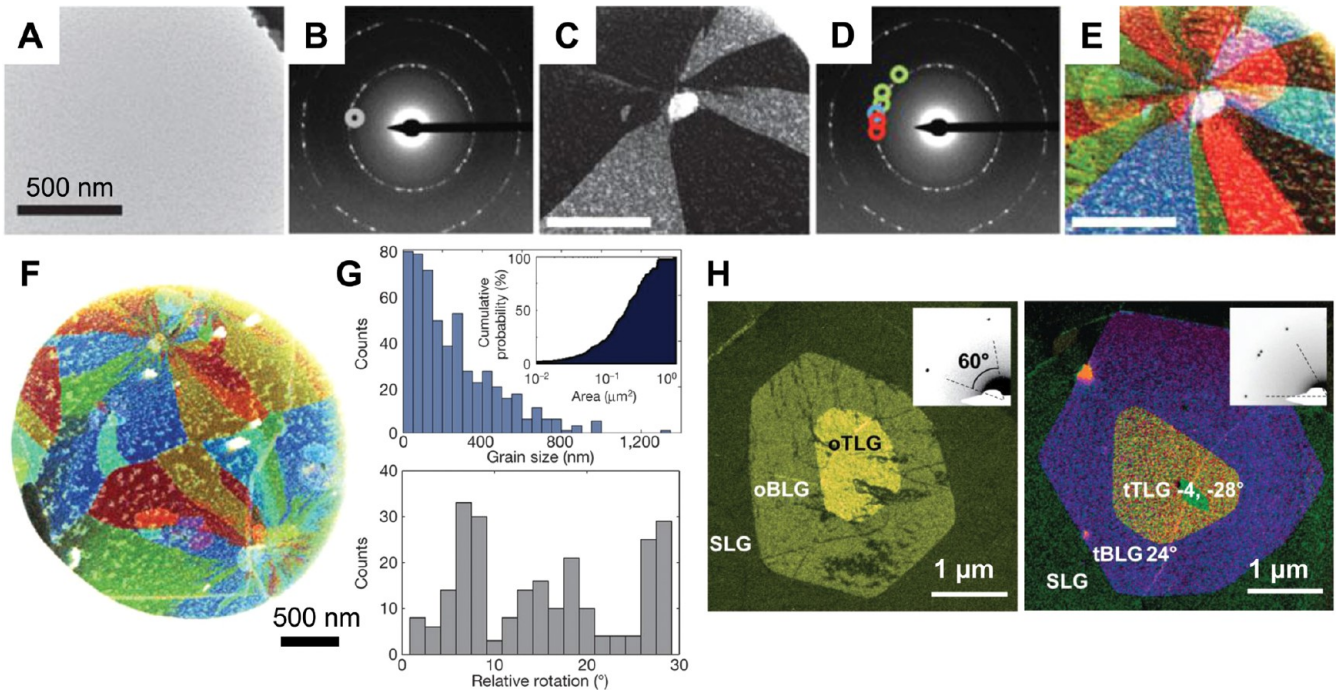

FIGURE 2. DF-TEM imaging of polycrystallinity in graphene. (A–E) DF-TEM process for characterization of graphene grain structure, resulting in (F) a color-coded large-scale image of various crystals in the graphene sheet. (G) Histograms of grain size (top) and relative rotation between grains (bottom). Adapted from ref 21. Copyright 2011 Nature Publishing Group. (H) DF-TEM images of multilayer regions with Bernal (left) and twisted (right) stacking. Inset shows the corresponding diffraction patterns. Adapted from ref 27. Copyright 2012 American Chemical Society.

growth, as well as their electrical and mechanical properties. We will also discuss the various structural behaviors of multilayered CVD graphene, and how they affect its optical properties. However, in order to understand the effects of such structures, one must first be able to accurately identify them. To this end, we begin by describing a transmission electron microscopy (TEM) technique that has recently been demonstrated to provide robust, large-area imaging of crystal orientations in CVD graphene films.

Large-Scale Structural Imaging with Dark-Field TEM

Many microscopy techniques have been applied to provide spatially resolved information about the structure of graphene. While high-resolution TEM (HR-TEM)[21,22] and scanning tunneling microscopy[23,24] can provide unrivaled atomic-scale images of the graphene lattice, they are slow and would require prohibitively long acquisition times to image a sample even on the micrometer scale. Other techniques for characterizing graphene with larger fields of view include Raman microscopy and low-energy electron microscopy (LEEM). While spatially resolved Raman spectroscopy is sensitive to the presence of defects in graphene,[25] it cannot determine the local crystal orientation of unstrained samples, and so results are difficult to interpret. On the other hand, LEEM yields diffraction information from the sample and can even be used to determine graphene's orientation relative to the substrate in situ;[26] however, its resolution is limited.

Coincidentally, TEM also possesses the capability to image in a configuration that is sensitive to electron diffraction. This imaging mode, named dark-field TEM (DF-TEM), is a robust method to image the different grain orientations in CVD graphene over large areas with high throughput.[21] The technique is also widely available, as it can be implemented even on microscopes which do not possess atomic resolution. The mechanism of DF-TEM can be understood from the top panels of Figure 2. In Figure 2A, Huang et al. show a typical TEM image of CVD graphene fully suspended on top of a hole, which exhibits almost no contrast differences across the sheet. The electron diffraction pattern from this area, however, shows many sets of 6-fold-symmetric spots (Figure 2B). Since a single crystal of graphene would yield one such set of diffracted spots due to the 6-fold symmetry of its lattice, this diffraction pattern implies that the area contains many distinct graphene crystals. In order to image this area in dark-field mode, one can place a small aperture in the diffraction plane to collect only the electrons passing

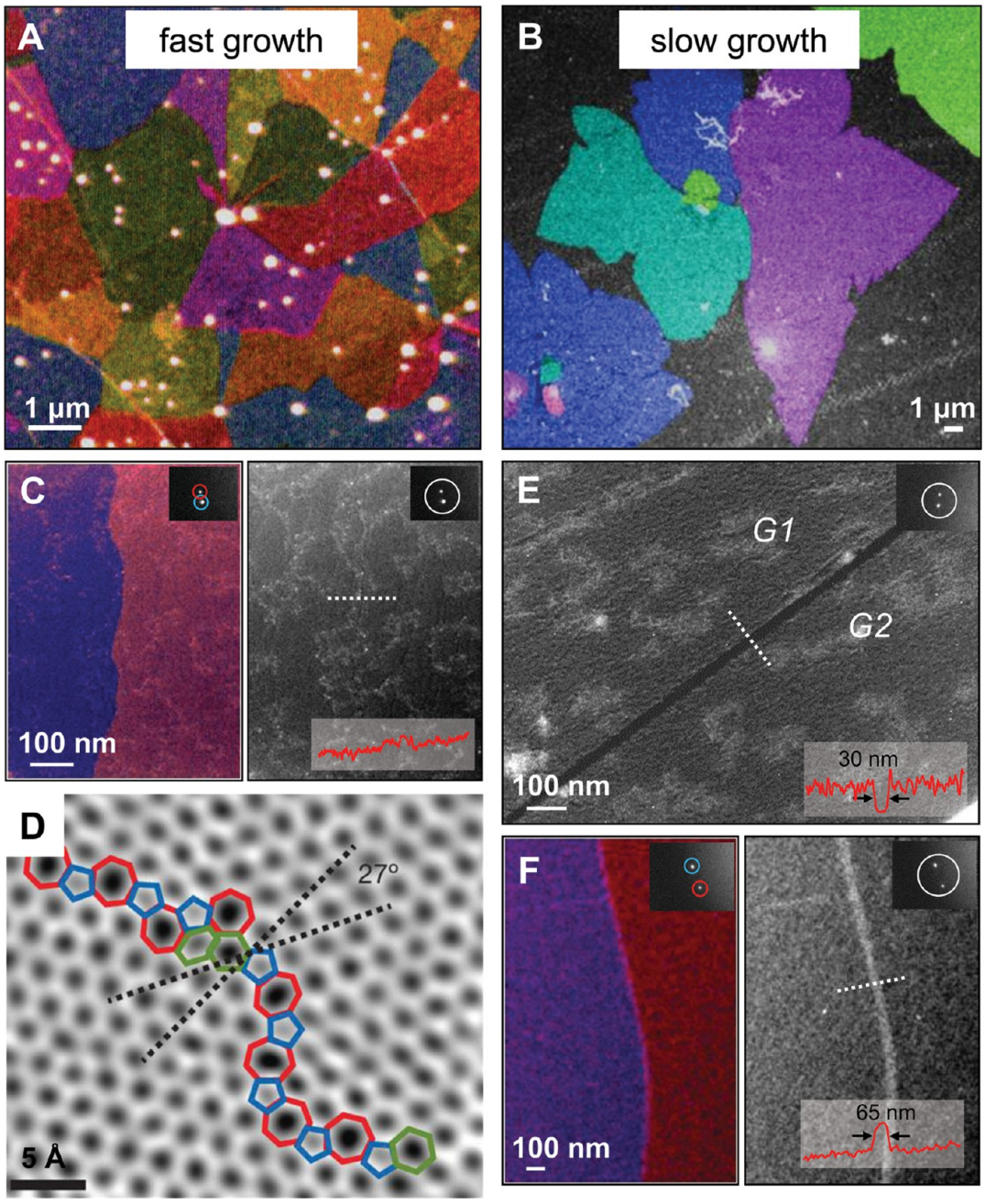

FIGURE 3. Imaging grain boundaries in graphene. DF-TEM images of (A) small grain and (B) large grain graphene. (C) A seamless grain boundary from the "fast" growth. Inset: diffraction spots and aperture locations used to take the DF-TEM image. (D) HR-TEM image of a grain boundary from the fast growth, showing planar stitching with aperiodic heptagon-pentagon pairs. DF-TEM images of (E) gapped and (F) overlapped grain boundaries from the slow growth, taken in the same manner as (C). Reproduced from refs 21 (Copyright 2011 Nature Publishing Group) and ref 28 (Copyright 2012 American Association for the Advancement of Science).

through it (denoted by white circle in Figure 2B), thereby selectively imaging the graphene domains diffracting in this small range of angles (Figure 2C). By repeating this process with several different aperture positions (Figure 2D), one can colorize and then overlay all the dark-field images to generate complete maps of the domain structure in this area (Figure 2E). Here, we see that many domains emerge from a common center, which could indicate that it was the location of a nucleation site. By performing DF-TEM over larger graphene areas, as in Figure 2F, the authors were able to quickly obtain statistical distributions of the sizes of individual domains, as well as the relative crystal orientation between adjacent domains (Figure 2G). In this particular sample, the mean domain size was 250 nm;

however, this parameter depends strongly on the synthesis conditions (see below). Also, this growth exhibited a preference for both low-angle (≈7°) and high-angle (≈30°) grain boundaries.

Finally, one can also determine the stacking orientations in multilayered CVD graphene with DF-TEM. In general, graphene layers can be vertically stacked either without interlayer rotation (Bernal or rhombohedral configurations) or with an arbitrary misorientation angle. It has been shown that both configurations can form naturally in graphene grown by CVD.[27] For example, in the left panel of Figure 2H, Brown et al. observed the local growth of three layers of graphene, which can be easily distinguished by their relative dark-field intensities. Since their combined electron diffraction pattern only contains one set of 6-fold symmetric spots, this indicates that the lattices of all the graphene layers were rotationally aligned. In contrast, the three distinct sets of diffraction spots in the right panel indicate that all three layers were misoriented.

Dark-Field TEM Characterization of Individual Grain Boundaries

Even without direct experimental evidence of the precise effects of grain boundaries in graphene, many groups have developed different CVD growth methods in order to obtain films with larger domain sizes.[11,19] Following these established procedures, our own group has studied the resulting graphene films in conjunction with DF-TEM,[28] and we shall discuss the findings for two such growths.

When graphene is synthesized with comparatively high reactant flow rates, the film nucleates and grows "fast", forming a continuous polycrystalline film with a relatively small average domain size of ≈1 μm (Figure 3A). However, when the Cu growth substrate was further enclosed in a pocket of Cu foil, gas flow and nucleation density were suppressed, and rate of growth substantially reduced.[11,19] In Figure 3B, this type of "slow" synthesis was stopped after only partial monolayer coverage in order to illuminate the flowered shapes of the graphene islands. Longer growth times, however, yielded more continuous films with domain sizes of ≈50 μm. Here, we see that a single graphene island actually contained several distinct domains, a finding similar to that of Wofford et al. using LEEM,[26] as well as small areas of BLG. These images reveal the complex structures that may arise even in seemingly simple graphene growth structures.

Despite the absence of atomic resolution, it is possible to use DF-TEM to study the morphology of individual grain boundaries. Figure 3C (left) shows a DF-TEM image of a grain boundary from the fast growth. Their diffraction spots are circled with their respective colors in the inset. On the right, both spots were selected simultaneously with the aperture, and the resulting dark-field image shows a seamless boundary. This suggests that the grain boundary formed an abrupt junction whose finer features cannot be resolved using DF-TEM. HR-TEM imaging performed on this type of growth, however, can provide images of grain boundaries with atomic detail. Figure 3D shows a micrograph of a 27° tilt boundary taken with an aberration-corrected scanning transmission electron microscope by Huang et al. Here, we see that the two domains have been connected by an aperiodic arrangement of pentagons, heptagons, and distorted hexagon defects. A similar structure has also been seen by Kim et al. on their samples.[22]

The slow growth, however, did not exhibit a tendency to form atomically abrupt interdomain connections. When the diffraction spots for two domains in this growth were selected simultaneously, Tsen et al. observed a crystalline discontinuity that was 30 nm wide, shown in Figure 3E. This suggests that this grain boundary could have been stitched together by an amorphous material. Additionally, adjacent domains were often observed to overlap each other instead of connecting in-plane (Figure 3F). Here, when imaging both spots, the BLG region appeared brighter, indicating that one domain extended 65 nm on top of the other. We can conclude from these images that the atomically abrupt boundary shown in Figure 3D is not universal, but rather the structure of grain boundaries in CVD graphene strongly depends on growth conditions.

The vast differences seen in the structure of grain boundaries should be directly manifested in their physical properties. To investigate the behavior of individual grain boundaries, DF-TEM provides an ideal platform for the imaging and identification of grain boundaries to be used in conjunction with other experimental methods.

Electrical Properties of Grain Boundaries

In general, grain boundaries in polycrystalline materials are expected to exhibit different electronic behaviors than the bulk material, which reflect their atomic arrangements. For graphene, it has been predicted that electrical transport across grain boundaries with perfectly periodic structures may be either highly transmissive or reflective over a wide range of energies, depending on the relative orientations of adjacent domains.[15] An example of such an extended defect has been experimentally identified using STM on graphene

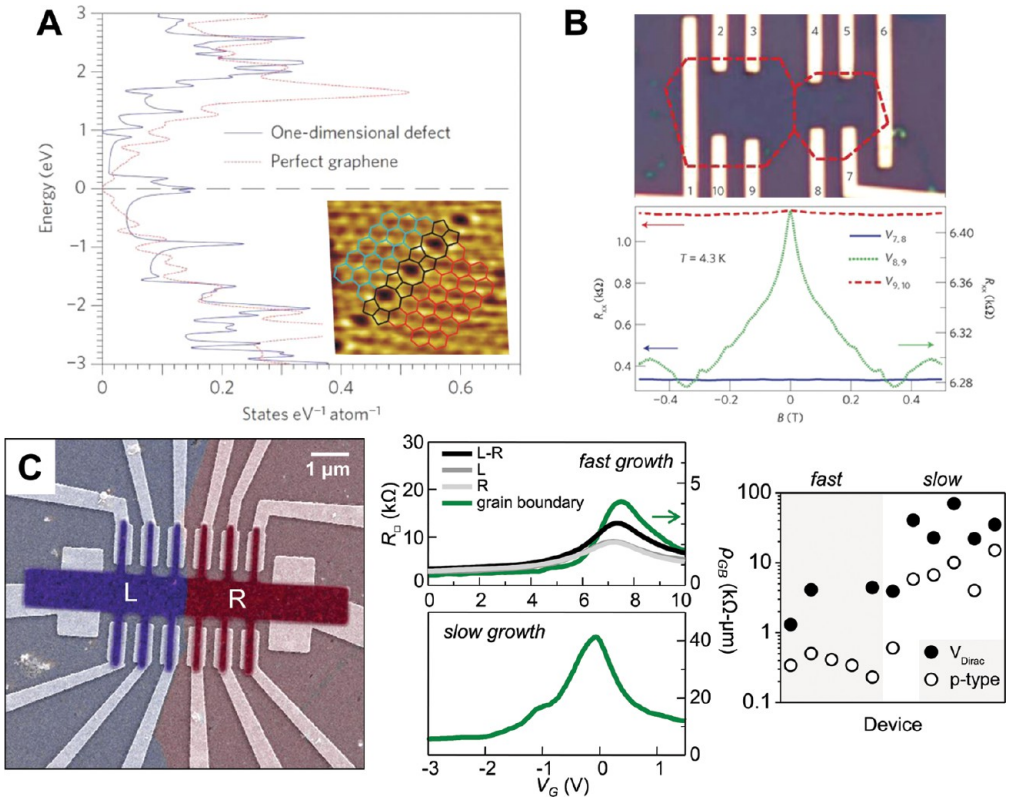

FIGURE 4. Electrical properties of grain boundaries. (A) Density of states for a "metallic" defect (blue) and for perfect graphene (red). Inset: STM image of the defect with superimposed structure. Adapted from ref 24. (B) Hall bar device fabricated over two joined graphene islands (top). Four-terminal magnetoresistance (R_{xx}) measured at 4.3 K within and across graphene islands. Interisland R_{xx} (dotted curve) displays a prominent weak localization peak. Adapted from ref 29. (C) (Left) Overlaid SEM/DF-TEM image showing a Hall bar device crossing a single grain boundary (GB). (Center) Gate-dependent four-terminal sheet resistance $R_\square$ and GB resistivity ρ_{GB} of device with single GB from fast (top) and slow (bottom) growths. (Right) ρ_{GB}, at V_{Dirac} and *p*-type doping, across 11 similar devices. Overall, GBs from the slow growth are an order of magnitude more resistive. Adapted from ref 28. Copyright 2012 American Association for the Advancement of Science.

grown on nickel, as its electronic density of states exhibited metallic character, in contrast to the semimetallic properties of the graphene sheet (Figure 4A).[24] As shown in the previous section, however, grain boundaries in CVD graphene may not form periodic defect structures even on the nanometer scale.[21,22] It is important to understand the electrical impact of realistic graphene grain boundaries and its implications for large-scale device transport.

Recently, Yu et al. synthesized graphene islands in the shape of polygons and inferred the locations of grain boundaries from islands that have merged.[29] Electrical measurements on these structures (Figure 4B) showed that interisland transport exhibited an increased resistance from that within an island, which they attributed to additional scattering caused by the grain boundary. Furthermore, magnetoresistance measurements across islands also demonstrated more prominent weak localization behavior. Ideally, however, electrical characterization of grain boundaries ought to be performed with simultaneous knowledge of the graphene's crystalline structure, especially since DF-TEM imaging has revealed that even single graphene islands may often be polycrystalline, making their precise domain structure difficult to predict a priori. Toward this end, Tsen et al. fabricated electrical chips with a fully suspended, electron transparent, thin silicon nitride membrane in the center.[28] Electron-beam lithography was used to pattern electrical devices consisting of individual grain boundaries that were first identified with DF-TEM. An example is shown in the left panel of Figure 4C. Here, the colorized DF-TEM image was overlaid on top of the SEM image of the device, showing that it crossed a single grain boundary. Graphene in the faded areas was etched away in a subsequent step.

The middle panel in Figure 4C shows the result of transport measurements performed across a grain boundary from the fast growth (as in Figure 3A). Resistance as a function of gate voltage exhibited nearly identical values for the left (L) and right (R) domains, whereas cross-domain resistance (L−R) was increased due to scattering from the

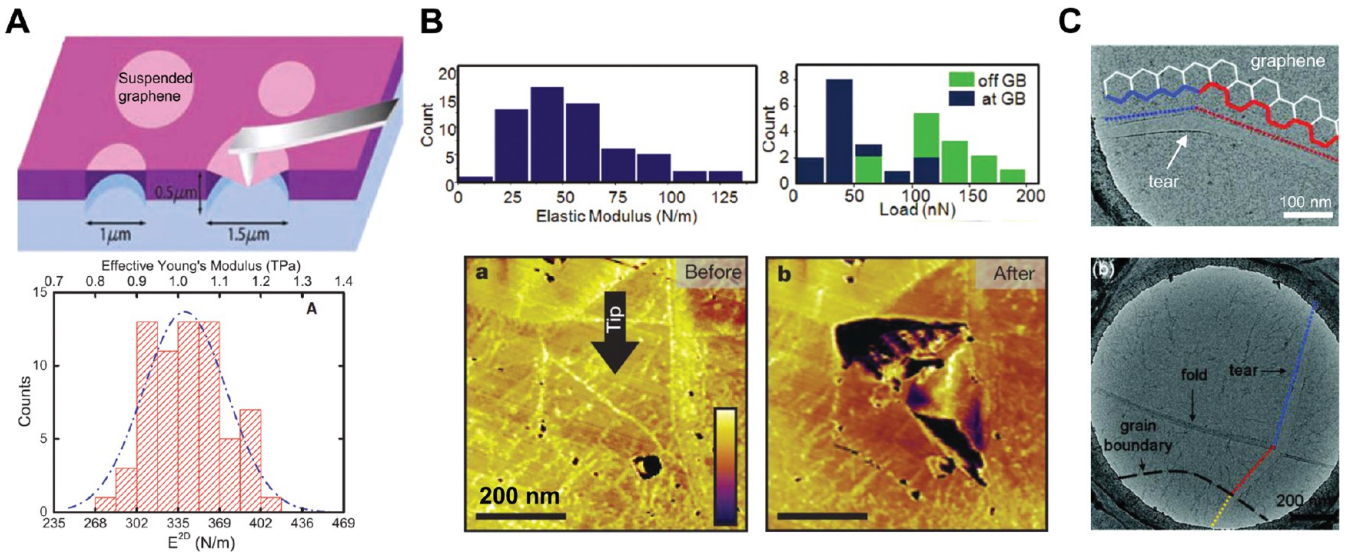

FIGURE 5. Mechanical properties of grain boundaries. (A) (Top) Schematic of nanoindentation measurements. (Bottom) Histograms of elastic stiffness of mechanically exfoliated graphene. Adapted from ref 4. (B) (Top) Histograms of elastic stiffness of CVD graphene (left) and breaking loads on and off the grain boundary (right), showing lower loads at the GB. (Bottom) AFM images before and after nanoindentation showing that tears occurred along the grain boundaries. Adapted from ref 21. Copyright 2011 Nature Publishing Group. (C) (Top) TEM image of a tear in suspended graphene. The red and blue dotted lines represent armchair and zigzag tear edges, respectively. (Bottom) TEM image of graphene tear crossing a grain boundary. Adapted from ref 32. Copyright 2012 American Chemical Society.

grain boundary. By subtracting the averaged L and R values from that of L−R, one can determine the absolute resistivity of the grain boundary itself, ρ_{GB}. Here, ρ_{GB} was gate tunable, from 0.5 k$\Omega\cdot\mu$m in the *p*-doped regime to 4 k$\Omega\cdot\mu$m at the Dirac point. The *p*-type resistivity value is also similar to the grain boundary resistivities reported by Jauregui et al. in their electrical measurements taken across and within graphene islands.[30] The same measurement on a grain boundary from the slow growth (Figure 4C, middle panel, bottom) yielded qualitatively similar results, although its resistivity was an order of magnitude greater at all gate voltages. Further measurements on a total of 11 grain boundaries from both growths confirmed this overall trend (right panel), indicating that the electrical properties of grain boundaries in CVD graphene are directly correlated with their structure. Tsen et al. further showed that well-stitched grain boundaries did not substantially decrease the overall conductance and carrier mobility for large-scale CVD graphene films, and their values can in principle can provide high performance, approaching 90% that of single-crystal graphene, even for films with a modest average domain size of ≈1 μm.

Mechanical Properties of Grain Boundaries

In contrast to their effects on electrical performance, even grain boundaries formed in highly reactive growth environments seem to greatly limit the mechanical strength of CVD graphene. Mechanical information can be obtained by suspending graphene on top of holes and performing nanoindentation measurements using the tip of an atomic force microscope (AFM) (Figure 5A, top panels). Such studies done on single-crystal, exfoliated graphene revealed an exceptionally strong material with a high elastic modulus (≈1 TPa) and large breaking force (≈2 μN) (Figure 5A, bottom panels).[4] This is largely a reflection of the strength of carbon−carbon bonds, the same concept that has previously motivated the use of carbon fibers to mechanically reinforce composite materials.

For polycrystalline graphene, earlier theoretical work has predicted that grain boundaries with perfectly periodic defect structures may exhibit a wide range of mechanical properties, depending on the relative tilt angle between adjacent domains.[16] In particular, grain boundaries with small tilt angles required the incorporation of defects with large initial strain, which then led to a significant reduction in their breaking strength when pulled in the direction perpendicular to the boundary. In contrast, defect structures in large angle boundaries were largely unstrained, and so were calculated to be just as strong as a pristine graphene sheet. However, indentation measurements performed on CVD graphene films revealed both their elastic modulus and breaking force to be consistently reduced by an order of magnitude from that of exfoliated graphene (Figure 5B, top panels).[31] While the softening of graphene's stiffness was attributed to the presence of ripples in the film and not to

grain boundaries, its breaking strength was severely weakened by its polycrystallinity. In fact, as shown in the bottom panels, CVD graphene was often observed to tear precisely along its grain boundaries, even for growth conditions which should provide good intergrain stitching. Here, grain boundaries were imaged using AFM phase, which has been shown to be directly correlated to their TEM-resolved structures.[21,31] On the other hand, Kim et al. have imaged suspended CVD graphene films with pre-existing tears using TEM, and found cracks to have propagated perpendicularly across a grain boundary, leaving the boundary unperturbed (Figure 5C).[32]

The substantial reduction in the overall mechanical strength of CVD graphene was attributed to several possible factors. First, the presence of larger voids in local areas along the grain boundary could have initiated fracture and have led to unzipping.[31] Also, AFM indentation most likely induced both shear and tensile forces at grain boundaries, the combined effect of which may have made them more mechanically vulnerable. Finally, it has been recently suggested that the intersection of two or more grain boundaries could actually be the weakest points in the film and therefore start its rupture.[17] Overall, these studies have demonstrated that the mechanical properties of CVD graphene are an area that still requires much further optimization in order to achieve the performance limits of exfoliated graphene.

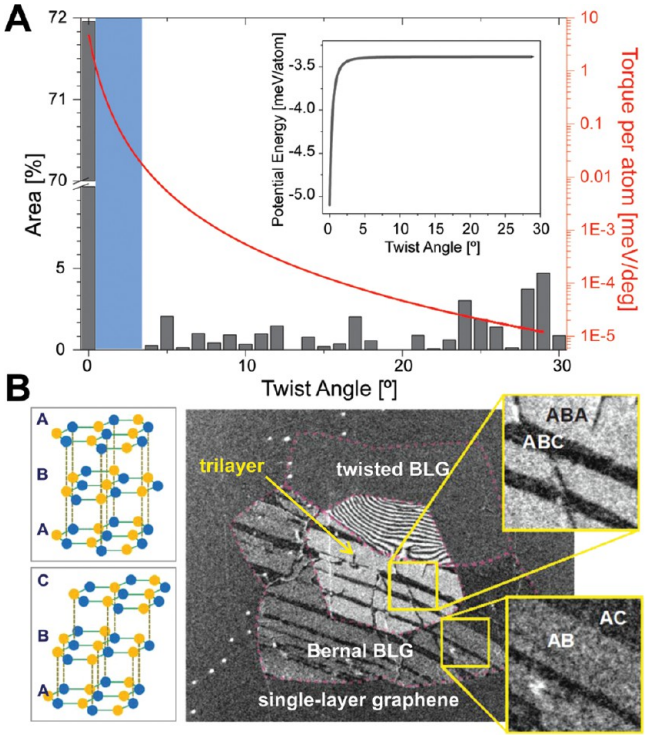

FIGURE 6. Stacking distribution in bilayer CVD graphene. (A) Area histogram of bilayer twist angle distribution. Torque (red) is calculated based on the theoretical interlayer potential (inset). (B) (Right) DF-TEM image of a three-layer system, showing AB to AC twinning in Bernal stacked bilayer and alternating ABA/ABC regions in oriented trilayer. Adapted from refs 27 (Copyright 2012 American Chemical Society), 33 (Copyright 2011 American Chemical Society), and 37.

Structure of Multilayer CVD Graphene

As we discussed above, CVD synthesis conditions can be tuned to produce large regions with multilayer graphene. By performing DF-TEM imaging over many multilayered areas, Brown et al. have found that over 70% of all BLG grown is stacked in the Bernal configuration, while the rest are rotated with a relative angle ranging from 4° to 30° (Figure 6A, main panel).[27] Interestingly, no twisted BLG was found with angles below 4°, which elucidates the energetics of the growth. There is a strong energetic preference for BLG to form with Bernal stacking (Figure 6A, inset), accounting for its prevalence in CVD synthesis. When BLG has begun to grow with a small interlayer rotation, there would be a large effective torque to drive the growth toward the Bernal configuration. However, this torque also exponentially decreases with increasing rotation angle, and so twisted BLG formed with large interlayer rotation is likely to remain as such for the entirety of the growth.

In addition to differences in twist angle, multilayered graphene grown by CVD also exhibits other structural variations. Figure 6B (right panel) shows a DF-TEM image of a triple-layered graphene structure. Here, the first layer consists of a single crystal. The second layer contains two domains: one Bernal-stacked with the first layer and another twisted by 5°. The third layer is again a single domain, with the same orientation as the first layer throughout. For the areas where all layers are rotationally aligned, we see abrupt striations in the DF-TEM image of bright and dark intensity corresponding to domains of alternate stacking in bilayer (AB/AC) and trilayer (ABA/ABC) graphene. As shown in the left panel, when layering graphene with the same orientation, there is a translational degree of freedom between the layers that gives rise to various stacking orders. Since each stacking order causes specific interference effects in the diffracted electron beam, the different stacking domains are manifested as bright and dark areas in the DF-TEM image. Recently, it has also been shown that micro-Raman imaging can also be used to differentiate and map stacking order in trilayer graphene.[33]

Finally, a different type of interference pattern was observed where the second layer is rotated. Here, while the first and third layers were approximately aligned, the twisted

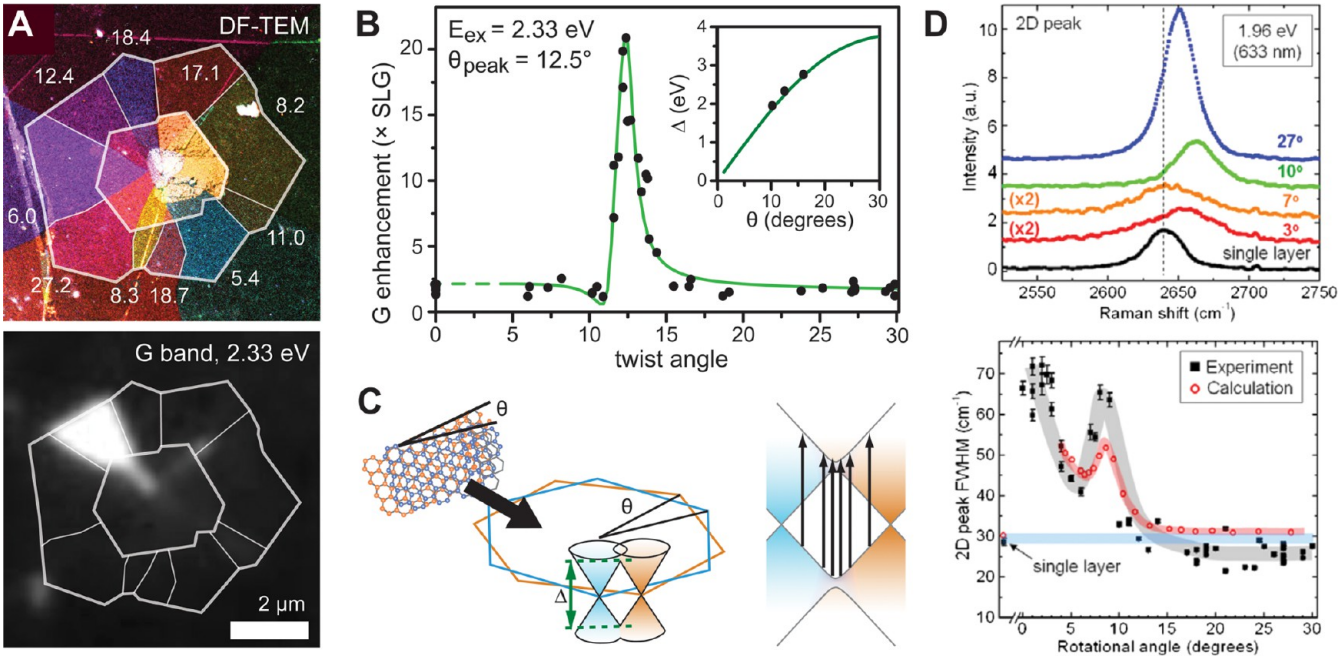

FIGURE 7. Raman enhancement in twisted BLG. (A) A DF-TEM image (top) and G band Raman image (bottom) illustrating strong G band enhancement for a 12.4° twisted bilayer domain. (B) Experimentally measured G band enhancement vs θ. (inset) Laser excitation energy vs twist angle corresponding to the maximum G band enhancement (points), fit to a theoretical plot of Δ vs θ (see panel C). (C) (Left) Band structure of twisted BLG for noninteracting layers. The Dirac cones from each layer (orange, blue) are rotated in k space by θ and intersect at an energy Δ. (Right) Schematic of the parallel band transition. Adapted from ref 35. Copyright 2012 American Chemical Society. (D) Raman 2D peak spectra of twisted BLG (top) and comparison of experimental and calculated values for 2D peak width as a function of θ (bottom). Similar calculations elucidated variations in the 2D peak intensity and position. Adapted from ref 36.

intermediate layer caused them to lose atomic registry on the micrometer scale. In contrast to the discrete intensity variations from oriented stacking domains, in this area we see oscillatory changes in intensity constituting an elaborate Moiré pattern, which originates from differences in local strain between the upper and lower layers that were likely produced during the growth and transfer processes.

The rich structural behaviors seen in multilayered graphene grown by CVD may also give rise to unique electronic and mechanical properties, in the same way that grain boundaries impart new properties to single-layer graphene. For instance, as discussed in the Introduction, Bernal-stacked BLG exhibits a bandgap that is tunable with a vertical electric field, while twisted BLG is gapless.[20] Junctions between twisted and Bernal-stacked BLG could also enable novel heterostructure devices, whereas the one-dimensional boundaries between BLG domains of different stacking orders could themselves exhibit unique electronic properties. This is a topic that is currently being explored by many groups, including our own, and so many of these effects are yet unknown.

While the structure of the π bands for twisted BLG resembles that of single-layer graphene close to the Dirac point, electronic interactions between the twisted layers manifest themselves at higher energies, which can be probed optically using Raman and absorption spectroscopy.

Optical Properties of Twisted Bilayer Graphene

Although a variety of interesting optical signatures have been observed in twisted BLG,[25,34] such studies have been hindered by the difficulty of determining the twist angle for a large sample size. As was the case for understanding the electronic and mechanical properties of grain boundaries in CVD graphene, precise, large-scale structural characterization has been invaluable for research in this area. Recent work combining TEM diffraction and Raman spectroscopy has allowed direct correlation between the optical properties of twisted BLG and twist angle (Figure 7A).[35,36] For given laser excitation energy, it was found that there is over an order of magnitude increase in the Raman G band intensity (Figure 7B), as well as a small increase in absorption, for a specific twist angle. The relationship between the twist angle corresponding to the peak G band intensity and the excitation energy is approximately linear over the

range probed experimentally (~6° and 0.8 eV; see Figure 7B, inset).

These unusual optical properties can be explained with a simple band-structure model. As discussed previously, the band-structure of single-layer graphene is approximately linear. In the low-energy limit, it consists of a set of cones which form a hexagon in momentum space (Figure 7C, left). To a first approximation, the band-structure of twisted BLG is simply two sets of these cones that are rotated in momentum space by the same twist angle (θ) as the real space layers (Figure 7C, left). Interesting phenomena occur near the energy where the cones from each layer meet, which is continuously tunable with θ from hundreds of meV at a few degrees to above 3 eV near 30° (Figure 7B, inset). The angle and energy where absorption and Raman enhancement are found to occur are well-described by the theoretically predicted energy where the bands from each layer meet.[35,36] An electronic splitting occurs at the avoided crossing of the Dirac cones from each layer, leading to a van Hove singularity in the density-of-states of twisted BLG. This has been observed with scanning tunneling spectroscopy (STS) at low twist angles.[23]

However, the origin of the interesting optical properties observed in twisted BLG is not the van Hove singularity observed with STS. Theoretical work by Havener et al. has shown that a new family of optical transitions is enabled in twisted BLG between the Dirac cones belonging to different layers. There is a large singularity in the joint density-of-states for such transitions, because the relevant bands run parallel to each other over many values of momentum (Figure 7C, right). By calculating the optical matrix element for all possible transitions in twisted BLG, it was shown that these "parallel band" transitions were primarily responsible for the observed enhancements in G band Raman intensity and absorption.[35] Full calculations of the Raman spectra by Kim et al., taking into account the tight-binding band structure, electron-photon, and electron−phonon interactions in twisted bilayer graphene, confirm a strong G band enhancement that matches experimental data. Their work also elucidates the origin of interesting variations in the Raman 2D bandwidth, position, and intensity as a function of twist angle (Figure 7D).[36]

The unique optical transitions in twisted BLG could have interesting implications for the optoelectronic properties of this material; for instance, it may be possible to optically pump electrons between layers at a specific energy determined by θ. In addition, the magnitude of the optical matrix element for parallel band transitions depends on the degree of coupling between layers, which in turn will affect the magnitude of the G band and optical absorption enhancement. This could allow future quantitative studies of the coupling between graphene layers under a variety of conditions, such as changes in temperature, pressure, or intercalation. Finally, the recently established correlation between structure and optical properties in twisted BLG can enable identification of the twist angle on arbitrary substrates, which in turn will allow further optical, electronic, and mechanical studies of this material as a function of twist angle in geometries which are not compatible with TEM characterization.

Conclusion

The development of large-scale graphene synthesis by CVD opens the door for its integration in device applications. Before this can be done effectively, however, we must have a clear understanding of its physical properties, especially regarding the material's polycrystallinity and sometimes multilayered structure, the most prominent differences seen from exfoliated graphene. DF-TEM is an ideal technique to image the crystalline orientations of CVD graphene films over large areas, which can furthermore be combined with other experimental methods to understand the electronic, mechanical, optical, and other physical properties of such structures. In particular, grain boundaries can be tailored during synthesis to have a minimal impact on the electrical properties of the film. While they currently reduce its mechanical strength by an order of magnitude from single-crystal exfoliates, the microscopic mechanism for this remains unclear, and further optimization may create grain boundaries with higher mechanical strength. Stacked graphene layers introduce additional degrees of freedom through variations in interlayer rotation angle and stacking order. In fact, both Bernal and twisted multilayer graphene is synthesized by the CVD process, and each exhibits unique structural and optical behaviors. Their mechanical and electronic properties, while still largely unknown, can in principle be studied using similar methods, which we also aim to address soon. We hope that a clear understanding of the various properties of CVD graphene will provide the necessary feedback to optimize its synthesis for relevant technologies in the future.

BIOGRAPHICAL INFORMATION

Adam W. Tsen is a Ph.D. candidate in Applied Physics at Cornell University. He received his B.S. degrees in Physics and Electrical Engineering at the University of California, Berkeley in 2006. His current research interest is in the spatially resolved characterization of electrical transport in carbon nanostructures.

Lola Brown is a Ph.D. candidate in Chemistry and Chemical Biology at Cornell University. She received her M.Sc. degree in Chemistry at Tel Aviv University, Israel. She is excited about *in situ* imaging and control of graphene structures.

Robin W. Havener received her BSE degree in Materials Science and Engineering from the University of Pennsylvania in 2008. Currently, she is a Ph.D. candidate in Applied Physics at Cornell University, researching optical imaging and spectroscopy of graphene.

Jiwoong Park is an Associate Professor in the Department of Chemistry and Chemical Biology at Cornell University, with a Ph.D. in Physics from the University of California, Berkeley. Before coming to Cornell University, he was a junior fellow of the Rowland Institute at Harvard University. His research interests focus on the electronic and optical properties of nanoscale materials including semiconductor nanowires, carbon nanotubes, and graphene.

FOOTNOTES

*To whom correspondence should be addressed. E-mail: jpark@cornell.edu.
The authors declare no competing financial interest.

REFERENCES

1 Geim, A. K. Graphene: status and prospects. *Science* **2009**, *324*, 1530–1534.

2 Castro Neto, A. H.; Peres, N. M. R.; Novoselov, K. S.; Geim, A. K. The electronic properties of graphene. *Rev. Mod. Phys.* **2009**, *81*, 109–162.

3 Nair, R. R.; Blake, P.; Grigorenko, A. N.; Novoselov, K. S.; Booth, T. J.; Stauber, T.; Peres, N. M. R.; Geim, A. K. Fine Structure Constant Defines Visual Transparency of Graphene. *Science* **2008**, *320*, 1308.

4 Lee, C.; Wei, X.; Kysar, J. W.; Hone, J. Measurement of the elastic properties and intrinsic strength of monolayer graphene. *Science* **2008**, *321*, 385–388.

5 Hass, J.; de Heer, W. A.; Conrad, E. H. The growth and morphology of epitaxial multilayer graphene. *J. Phys.: Condens. Matter* **2008**, *20*, 323202.

6 Waldmann, D.; Jobst, J.; Speck, F.; Seyller, T.; Krieger, M.; Weber, H. B. Bottom-gated epitaxial graphene. *Nat. Mater.* **2011**, *10*, 357–360.

7 Dreyer, D. R.; Park, S.; Bielawski, C. W.; Ruoff, R. S. The chemistry of graphene oxide. *Chem. Soc. Rev.* **2010**, *39*, 228–240.

8 Reina, A.; Jia, X.; Ho, J.; Nezich, D.; Son, H.; Bulovic, V.; Dresselhaus, M. S.; Kong, J. Large area, few-layer graphene films on arbitrary substrates by chemical vapor deposition. *Nano Lett.* **2009**, *9*, 30–35.

9 Li, X.; Cai, W.; An, J.; Kim, S.; Nah, J.; Yang, D.; Piner, R.; Velamakanni, A.; Jung, I.; Tutuc, E.; Banerjee, S. K.; Colombo, L.; Ruoff, R. S. Large-area synthesis of high-quality and uniform graphene films on copper foils. *Science* **2009**, *324*, 1312–1314.

10 Kim, K. S. Large-scale pattern growth of graphene films for stretchable transparent electrodes. *Nature* **2009**, *457*, 706–710.

11 Li, X.; Magnuson, C. W.; Venugopal, A.; Tromp, R. M.; Hannon, J. B.; Vogel, E. M.; Colombo, L.; Ruoff, R. S. Large-area graphene single crystals grown by low-pressure chemical vapor deposition of methane on copper. *J. Am. Chem. Soc.* **2011**, *133*, 2816–2819.

12 Mattevi, C.; Kim, H.; Chhowalla, M. A review of chemical vapour deposition of graphene on copper. *J. Mater. Chem.* **2011**, *21*, 3324–3334.

13 Bae, S.; Kim, H.; Lee, Y.; Xu, X.; Park, J.-S.; Zheng, Y.; Balakrishnan, J.; Lei, T.; Kim, H. R.; Song, Y. I.; Kim, Y.-J.; Kim, K. S.; Ozyilmaz, B.; Ahn, J.-H.; Hong, B. H.; Iijima, S. Roll-to-roll production of 30-in. graphene films for transparent electrodes. *Nature Nanotechnol.* **2010**, *5*, 574–8.

14 Levendorf, M. P.; Ruiz-Vargas, C. S.; Garg, S.; Park, J. Transfer-free batch fabrication of single layer graphene transistors. *Nano Lett.* **2009**, *9*, 4479–4483.

15 Yazyev, O. V.; Louie, S. G. Electronic transport in polycrystalline graphene. *Nat. Mater.* **2010**, *9*, 806–809.

16 Grantab, R.; Shenoy, V. B.; Ruoff, R. S. Anomalous Strength Characteristics of Tilt Grain Boundaries in Graphene. *Science* **2010**, *330*, 946–948.

17 Kotakoski, J.; Meyer, J. Mechanical properties of polycrystalline graphene based on a realistic atomistic model. *Phys. Rev. B* **2012**, *85*, 195447.

18 Malola, S.; Häkkinen, H.; Koskinen, P. Structural, chemical, and dynamical trends in graphene grain boundaries. *Phys. Rev. B* **2010**, *81*, 165447.

19 Vlassiouk, I.; Regmi, M.; Fulvio, P.; Dai, S.; Datskos, P.; Eres, G.; Smirnov, S. Role of hydrogen in chemical vapor deposition growth of large single-crystal graphene. *ACS Nano* **2011**, *5*, 6069–6076.

20 Lopes dos Santos, J. M. B.; Peres, N. M. R.; Castro, A. H. Graphene bilayer with a twist: Electronic structure. *Phys. Rev. Lett.* **2007**, *99*, 256802.

21 Huang, P. Y.; Ruiz-Vargas, C. S.; van der Zande, A. M.; Whitney, W. S.; Levendorf, M. P.; Kevek, J. W.; Garg, S.; Alden, J. S.; Hustedt, C. J.; Zhu, Y.; Park, J.; McEuen, P. L.; Muller, D. A. Grains and grain boundaries in single-layer graphene atomic patchwork quilts. *Nature* **2011**, *469*, 389–392.

22 Kim, K.; Lee, Z.; Regan, W.; Kisielowski, C.; Crommie, M. F.; Zettl, A. Grain boundary mapping in polycrystalline graphene. *ACS Nano* **2011**, *5*, 2142–2146.

23 Li, G.; Luican, A.; Lopes dos Santos, J. M. B.; Castro Neto, A. H.; Reina, A.; Kong, J.; Andrei, E. Y. Observation of Van Hove singularities in twisted graphene layers. *Nat. Phys.* **2009**, *6*, 109–113.

24 Lahiri, J.; Lin, Y.; Bozkurt, P.; Oleynik, I. I.; Batzill, M. An extended defect in graphene as a metallic wire. *Nat. Nanotechnol.* **2010**, *5*, 326–329.

25 Malard, L. M.; Pimenta, M. A.; Dresselhaus, G.; Dresselhaus, M. S. Raman spectroscopy in graphene. *Phys. Rep.* **2009**, *473*, 51–87.

26 Wofford, J. M.; Nie, S.; McCarty, K. F.; Bartelt, N. C.; Dubon, O. D. Graphene Islands on Cu Foils: The Interplay between Shape, Orientation, and Defects. *Nano Lett.* **2010**, *10*, 4890–4896.

27 Brown, L.; Hovden, R.; Huang, P.; Wojcik, M.; Muller, D. A.; Park, J. Twinning and twisting of tri- and bilayer graphene. *Nano Lett.* **2012**, *12*, 1609–1615.

28 Tsen, A. W.; Brown, L.; Levendorf, M. P.; Ghahari, F.; Huang, P. Y.; Havener, R. W.; Ruiz-Vargas, C. S.; Muller, D. A.; Kim, P.; Park, J. Tailoring Electrical Transport Across Grain Boundaries in Polycrystalline Graphene. *Science* **2012**, *336*, 1143–1146.

29 Yu, Q.; Jauregui, L. A.; Wu, W.; Colby, R.; Tian, J.; Su, Z.; Cao, H.; Liu, Z.; Pandey, D.; Wei, D.; Chung, T. F.; Peng, P.; Guisinger, N. P.; Stach, E. A.; Bao, J.; Pei, S.-S.; Chen, Y. P. Control and characterization of individual grains and grain boundaries in graphene grown by chemical vapour deposition. *Nat. Mater.* **2011**, *10*, 443–449.

30 Jauregui, L. A.; Cao, H.; Wu, W.; Yu, Q.; Chen, Y. P. Electronic properties of grains and grain boundaries in graphene grown by chemical vapor deposition. *Solid State Commun.* **2011**, *151*, 1100–1104.

31 Ruiz-Vargas, C. S.; Zhuang, H. L.; Huang, P. Y.; van der Zande, A. M.; Garg, S.; McEuen, P. L.; Muller, D. A.; Hennig, R. G.; Park, J. Softened elastic response and unzipping in chemical vapor deposition graphene membranes. *Nano Lett.* **2011**, *11*, 2259–2263.

32 Kim, K.; Artyukhov, V. I.; Regan, W.; Liu, Y.; Crommie, M. F.; Yakobson, B. I.; Zettl, A. Ripping graphene: preferred directions. *Nano Lett.* **2012**, *12*, 293–297.

33 Lui, C. H.; Li, Z.; Chen, Z.; Klimov, P. V.; Brus, L. E.; Heinz, T. F. Imaging stacking order in few-layer graphene. *Nano Lett.* **2011**, *11*, 164–169.

34 Ni, Z.; Liu, L.; Wang, Y.; Zheng, Z.; Li, L.-J.; Yu, T.; Shen, Z. G-band Raman double resonance in twisted bilayer graphene: Evidence of band splitting and folding. *Phys. Rev. B* **2009**, *80*, 125404.

35 Havener, R. W.; Zhuang, H.; Brown, L.; Hennig, R. G.; Park, J. Angle-Resolved Raman Imaging of Interlayer Rotations and Interactions in Twisted Bilayer Graphene. *Nano Lett.* **2012**, *12*, 3162–3167.

36 Kim, K.; Coh, S.; Tan, L.; Regan, W.; Yuk, J.; Chatterjee, E.; Crommie, M.; Cohen, M.; Louie, S.; Zettl, A. Raman Spectroscopy Study of Rotated Double-Layer Graphene: Misorientation-Angle Dependence of Electronic Structure. *Phys. Rev. Lett.* **2012**, *108*, 246103.

37 Morell, E. S.; Vargas, P.; Chico, L.; Brey, L. Charge redistribution and interlayer coupling in twisted bilayer graphene under electric fields. *Phys. Rev. B* **2011**, *84*, 195421.